Programming function into mechanical forms by directed assembly of silk bulk materials

Benedetto Marelli[a,1], Nereus Patel[a], Thomas Duggan[a], Giovanni Perotto[a], Elijah Shirman[a], Chunmei Li[a], David L. Kaplan[a,b], and Fiorenzo G. Omenetto[a,c,d,2]

[a]Silklab, Department of Biomedical Engineering, Tufts University, Medford, MA 02155; [b]Department of Chemical Engineering, Tufts University, Medford, MA 02155; [c]Department of Electrical Engineering, Tufts University, Medford, MA 02155; and [d]Department of Physics, Tufts University, Medford, MA 02155

Edited by David A. Weitz, Harvard University, Cambridge, MA, and approved November 21, 2016 (received for review July 23, 2016)

We report simple, water-based fabrication methods based on protein self-assembly to generate 3D silk fibroin bulk materials that can be easily hybridized with water-soluble molecules to obtain multiple solid formats with predesigned functions. Controlling self-assembly leads to robust, machinable formats that exhibit thermoplastic behavior consenting material reshaping at the nanoscale, microscale, and macroscale. We illustrate the versatility of the approach by realizing demonstrator devices where large silk monoliths can be generated, polished, and reshaped into functional mechanical components that can be nanopatterned, embed optical function, heated on demand in response to infrared light, or can visualize mechanical failure through colorimetric chemistries embedded in the assembled (bulk) protein matrix. Finally, we show an enzyme-loaded solid mechanical part, illustrating the ability to incorporate biological function within the bulk material with possible utility for sustained release in robust, programmably shapeable mechanical formats.

assembly | silk | sol–gel | biomaterials | bioinspired

Biomimicry draws inspiration from multiple material functions (e.g., antibacterial and antifouling, light manipulation, heat dissipation, water sequestration, superhydrophobicity, adhesiveness, and enhanced mechanical properties) to develop universal fabrication strategies to design new structural materials with utility in a variety of fields ranging from the biomedical, to the technological and architectural. Naturally occurring materials are generated through a bottom-up "generative" process that involves a nontrivial interplay of mechanisms acting across scales from the atomic to the macroscopic. In this context, the assembly of structural biopolymers, the fundamental building blocks of natural materials, leads to hierarchically organized architectures that impart unique functionality to the end material formats.

Among the several structural proteins that have been studied, silk fibroin was recently shown to be suited for the generation of a number of biopolymer-based advanced material formats leveraging control of form (through sol–gel–solid transitions) and function (through material modification). The ability to generate functional materials based on water-based silk assembly is predicated on the control of the sol–gel–solid transitions of silk fibroin materials in ambient conditions. In Fig. 1*A*, the formation of 3D silk fibroin constructs is depicted through its dimensional hierarchy, from the nano- to the macroscales. Silk is extracted from natural sources (i.e., *Bombyx mori* cocoons) with a previously developed protocol (1) that yields a water suspension of the fibroin protein, where the protein molecules are organized in nanoscopic micelles (or nanoparticles) (top row of Fig. 1*A*), with an average diameter that changes as a function of concentration and molecular weight (Fig. S1).

Control over the dynamics of water evaporation regulates silk-fibroin assembly at the molecular level and the end-material format properties. This has been previously observed for natural silk in caterpillars and spiders and for a variety of other formats such as films, gels, sponges, and fibers (2–9). In particular, three different models have been proposed for silk assembly, which have been supported by diverse experimental evidences obtained from *Bombyx mori* silk, spider silk proteins, regenerated silk fibroin, and recombinantly produced spider silk proteins at different concentrations (9–18). A recent review covers in detail these models (19). (*i*) The first mechanism involves the formation of micellar nanostructures that fuse together via coalescence, forming microscopic globular structures that, in the presence of shear stress, elongate and fuse together (9). (*ii*) In a second theory, silk suspensions at high concentrations (close to precipitation) are considered as crystalline liquids that organize in nematic and hexagonal columnar phases (16). Liquid-crystal phases play a pivotal role in the formation of many biological systems (20, 21). A combination of shear thinning, changes in ion concentration, and molecular bending would then lead to assembly. (*iii*) A third model proposes a nucleation–aggregation mechanism, which is similar to the aggregation process reported for amyloid fibril formation (17, 22). Early β-sheet structures act as precursor (or nuclei) for the formation of ordered, energetically favored structures and template the molecular assembly. Nucleation–aggregation mechanisms are generally slow; thus, this model might apply when silk assembly occurs in a long time window. Nonetheless, the aforementioned mechanisms are based on sol–gel–solid transitions of silk proteins. For silk monoliths fabrication, this can be achieved in several ways, namely by (*i*) spontaneous

Significance

Engineering multiple functions in a single material format is a key design parameter to fabricate devices that can perform at the confluence between biology and technology. This can be achieved by designing materials with hierarchical structures across several scales or by embedding active molecules at the point of material formation. These approaches have been successfully pursued to engineer 2D materials formats. However, current technologies have limited the formation of 3D constructs with orthogonal functions. In this study, we demonstrate an entirely water-based sol–gel–solid process to generate 3D mechanical forms that embed biological (and other) functions. This approach is a step toward the development of multifunctional devices that may liaise between the biotic and abiotic worlds.

Author contributions: B.M. and F.G.O. designed research; B.M., N.P., T.D., G.P., and E.S. performed research; B.M. and C.L. contributed new reagents/analytic tools; B.M., N.P., G.P., E.S., D.L.K., and F.G.O. analyzed data; and B.M., D.L.K., and F.G.O. wrote the paper.

Conflict of interest statement: B.M., C.L., D.L.K., and F.G.O. are listed as inventors in a US patent application based on the technology described in this study.

This article is a PNAS Direct Submission.

See Commentary on page 428.

[1]Present address: Department of Civil and Environmental Engineering, Massachusetts Institute of Technology, Cambridge, MA 02139-4307.

[2]To whom correspondence should be addressed. Email: fiorenzo.omenetto@tufts.edu.

This article contains supporting information online at www.pnas.org/lookup/suppl/doi:10.1073/pnas.1612063114/-/DCSupplemental.

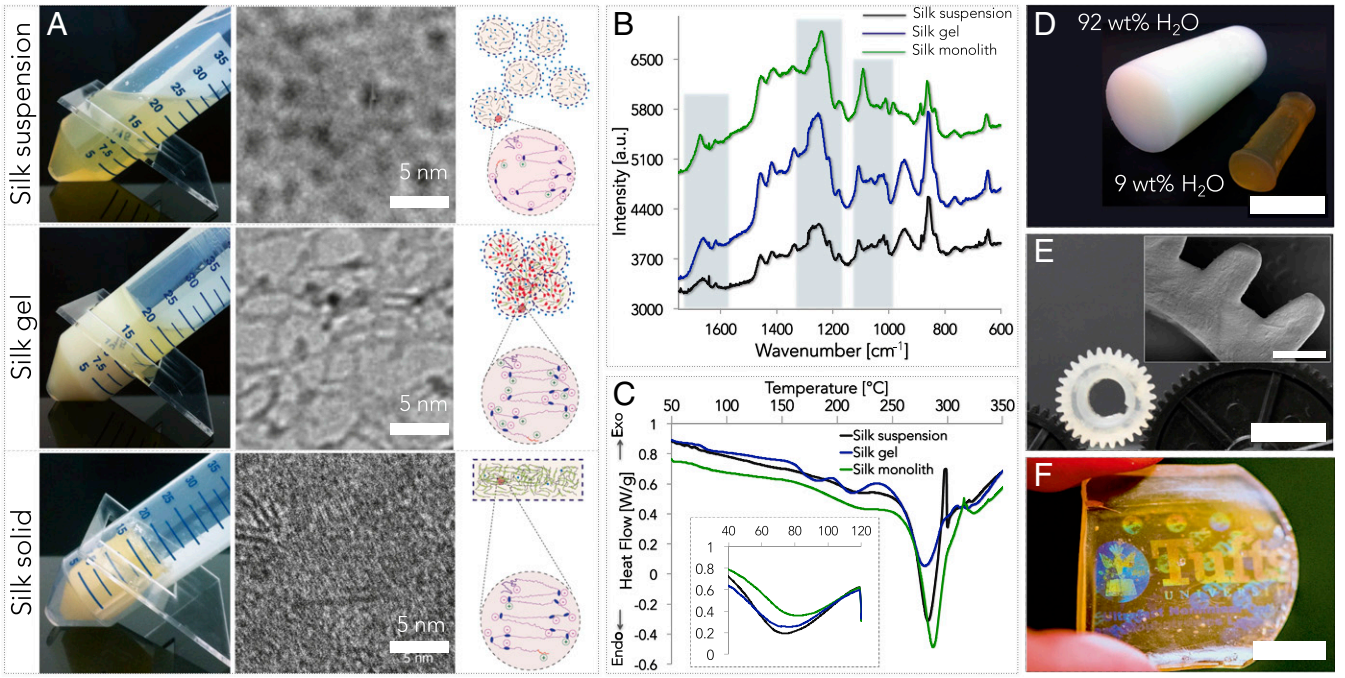

Fig. 1. Formation of 3D silk fibroin constructs through an all-water process. During self-assembly, the protein undergoes polymorphic changes that encompass its nanostructure, molecular configuration, and bound water. (*A*) Macroscopic and nanoscopic investigation of the self-assembly process and relative schematic of the proposed mechanism. Cryo-electron micrographs obtained at different stages of silk fibroin self-assembly depicted that the protein possesses (*i*) micellar (or nanoparticle), (*ii*) nanofibrillar, and (*iii*) bulk structures when in suspension, gel, and solid forms, respectively. β-Sheets configurations are visible in the micrograph of solid silk. The presented images were cropped from the original EM micrographs to highlight—with comparable resolution—the morphological changes at the nanoscale of silk fibroin materials during the sol–gel–solid transition. (*B*) Micro-Raman spectroscopy showed the polymorphic nature of the protein, which is organized in random coil, helices, and β-sheets when in suspension, gel, and solid form, respectively. (*C*) DSC showed a decrease in free water (endothermic peak decrease and shift toward higher temperature in the *Inset* image), a more crystalline configuration (decreased endothermic peaks in $T = 150–240$ °C range that mark amorphous-to-crystalline reconfiguration of the protein secondary structure), and an increase in the thermal stability (shift toward higher temperature of the endothermic peak in the $T = 250–300$ °C range, which mark protein degradation) of silk fibroin as the self-assembly progresses. (*D*) Gel–solid transition of silk fibroin materials is due to the evaporation of the free water present in the gel structure and results in a quasi-homogeneous shrinkage of the material. Volume reduction varies from 72 to 90%, depending on the initial concentration of the protein in the gel. (*E*) By using the homogenous volume reduction of the material during the gel–solid transition, complex shapes (e.g., gears) of defined dimensions can be fabricated, starting from appositely fabricated molds, that take into account the percentage of volume reduction. (*F*) Soft lithography techniques may also be used to microstructure the surface of silk solid materials during the gel–solid transition. For example, by compressing ($P = 100$ kPa) one surface of the gel to a nanostructured material during the gel–solid transition it is possible to replicate (as a negative) the holographic pattern present on the master.

assembly by leaving the suspension unperturbed for several weeks, (*ii*) water evaporation-driven assembly achieved with slow drying of the silk fibroin suspension for several days, (*iii*) directed assembly of silk fibroin molecules through electrogelation (23), which accelerates the process to few hours. The three methods yield silk fibroin gels of different nanoscale and microscale characteristics, as previously reported, which ultimately affect the structural properties of the silk solids (24). In particular, gels are formed by colloidal assembly of silk fibroin in microparticles, nanomatrices (second row of Fig. 1*A*), and nanoparticles for gel obtained via spontaneous self-assembly, slow drying, and electrogelation, respectively. Silk fibroin hydrogels are composed of a solid phase and of water. The interplay between silk fibroin and water in the gel structure can be described by the presence of free water, freezing bound water, and nonfreezing bound water (25). The gel–solid transition of silk fibroin materials to generate silk monoliths is achieved through evaporation of the free water present in the gel structure. During this two-step assembly process, silk fibroin molecules undergo polymorphic changes that affect the material nanostructure, molecular configuration, and amount of bound water. These different silk fibroin polymorphs were investigated during the assembly process to better understand the mechanism of silk fibroin assembly in 3D monolithic constructs.

Results and Discussion

Cryogenic transmission electron microscopy (cryo-TEM) was used to study silk fibroin morphology during the assembly process. The micrographs obtained at different assembly stages depict that the protein possesses micellar (or nanoparticle), nanofibrillar, and bulk structures when in suspension, gel, and solid forms, respectively (Fig. 1*A*). Limitations in the cryo-TEM technology did not allow to investigate silk fibroin conformation in suspension at concentrations higher than 1%. Indeed, the micellar (or nanoparticle) form might not be maintained at the point of sol–gel transition. β-Sheets configurations are visible in the cryo-TEM image of solid silk. Conformational changes during the sol–gel–solid transition were also characterized with micro-Raman spectroscopy (Fig. 1*B*). In particular, the study of the Raman shifts in the Amide I (1,700–1,600 cm^{-1}), Amide III (1,350–1,190 cm^{-1}), and C–C backbone (1,150–970 cm^{-1}) regions was used to investigate how the phase change of silk fibroin materials from solution to gel and solid forms was accompanied by conformational changes of the protein secondary and tertiary structures from random coil (Raman shift peaks at 1,640, 1,260, and 1,120 cm^{-1}) to helices (Raman shift peaks at 1,660, 1,240, and 1,130 cm^{-1}) and β-sheets (Raman shift peaks at 1,622, 1,230, and 1,150 cm^{-1}), respectively (26–28). The interplay between silk fibroin and water during the material fabrication process was investigated through differential scanning calorimetry (DSC) (Fig. 1*C*). The thermograms show a decrease in free water (endothermic peak decrease and shift toward higher temperature in the *Inset* image), increase in crystalline configuration (decrease of endothermic peaks in the $T = 150–240$ °C range that mark amorphous-to-crystalline reconfiguration of the protein secondary structure), and an

increase in the thermal stability (shift toward higher temperature of the endothermic peak in the T = 250–300 °C range, which mark protein degradation) of silk fibroin as the self-assembly progresses (29).

The free-water evaporation in the gel–solid transition results in a quasi-homogeneous shrinkage of the material with a volume reduction that varies from 72 to 90%, depending on the initial amount of water in the gel (Fig. 1*D*). Although this phenomenon has been largely reported for the formation of silk fibroin films and membranes, there was no indication before this study that bulk materials could be achieved with a similar methodology. Particularly surprising is the fact that the gel–solid transition yields a silk fibroin material with a predominance of β-sheet structures (sometimes referred to as "crystalline silk fibroin"). This is different from what happens during the formation of films by drop cast (7, 8) or of membranes by dip coating (30). In these two processes, a quasistatic water evaporation combined with an unperturbed silk fibroin suspension drives the removal of water and the corresponding formation of intermolecular and intramolecular hydrogen bonds without affecting the fibroin random coil configuration present in the solvated state. Concurrently, we have previously shown that the formation of films through a combination of water evaporation and electrogelation induced the reconfiguration of fibroin into β-sheet structures (31). Thus, the assembly of bulk silk materials is not reversible in water, as the β-sheet structures possess a very slow degradation rate in water environments. We tried to monitor the role of structural water in the gel–solid transition with attenuated total reflectance–Fourier transform infrared (FTIR) spectroscopy by replacing water (H_2O) with heavy water [deuterium oxide (D_2O)] in the silk water suspension. However, we have not been able to generate—for the gel format—an FTIR spectrum with a signal-to-noise ratio sufficient to unequivocally perform the spectroscopic analysis. Thus, we chose to monitor over time (during the gel–solid transition) the Amide III band (1,300–1,190 cm^{-1}) and the I_{850}/I_{830} ratio of silk gels' Raman spectra to investigate the role of structural water during assembly. In particular, the I_{850}/I_{830} ratio allows to study the hydrogen-bonding state of protein's tyrosine phenoxyl group—a more hydrophobic tyrosine environment (i.e., reduction of structural water in the protein) corresponds to higher I_{850}/I_{830} ratio (25, 32). The analysis of the Amide III scattering showed a Raman shift to lower wavenumbers during the water evaporation process, which is an indication of increased β-sheet formation during the gel–solid process (26, 27). The study of the I_{850}/I_{830} ratio during the gel–solid transition showed that the ratio increased during water evaporation, which can be considered as an indication of increased structural hydrophobicity that can be correlated with a more "crystalline" silk configuration. Complex shapes (e.g., gears) of defined dimensions can be obtained from appropriately fabricated molds that take into account the percentage of volume reduction (Fig. 1*E* and Fig. S2), thereby avoiding mechanical stresses from machining. Pressure-assisted soft lithography techniques may also be used to obtain microstructured and nanostructured features on the surface of silk solid materials during the gel–solid transition (2). This was shown by compressing at room temperature (P = 100 kPa, T = 22 °C) one surface of the gel onto a nickel holographic shim during the gel–solid transition and obtaining a negative replica of the master surface hologram (Fig. 1*F*).

The semicrystalline nature of silk fibroin and the presence of free and bound water in the protein structure impart partial thermoplasticity and thermorelaxation properties to the solid material (Fig. 2), as already reported for other structural proteins (33, 34). This is of potential interest to controllably deform and reshape the materials on the macroscale, adding increased utility to the solid silk formats. Thermogravimetric analysis was used to study the interplay between silk fibroin molecular weight and the residual water present in the solid material (Fig. 2*A*). The weight loss of silk materials as a function of temperature is caused by the evaporation of free water in the 100 °C region, of freezing bound water in the 150–240 °C region, and of the nonfreezing bound water above the degradation temperature of 270 °C. Any weight loss above 300 °C is due to protein pyrolysis. Thermogravimetric curves of silk fibroin showed an increase in free and bound water for materials with higher molecular weight. Micro-Raman spectroscopy was also used in this case to investigate the presence of structural water in solid silk materials, as a function of molecular weight (Fig. 2*B*). Although the spectra of the protein did not present significant differences in the Raman shift as a function of molecular weight, the measured I_{850}/I_{830} ratio (*Inset*) showed a more hydrophobic tyrosine environment (higher I_{850}/I_{830} ratio) for higher protein molecular weights (25, 32). As a proof-of-concept of silk fibroin thermoplasticity, a dead load of 200 g was applied to one end of a 2-cm-long silk rod (Ø = 1 mm) that was secured at the opposite end to a bench vise and heated with a heat gun (Fig. 2*C*). Thermographs of the experimental setup showed that the increase of the rod internal temperature above 60 °C induced a plastic deformation of the material. The partial thermoplasticity of silk fibroin materials at temperature above 60 °C may also be used to impart temperature-induced microreflow of the material surface enabling micro- and nanoimprinting of microstructures with a combination of heat and pressure. As a proof-of-concept, a 300 lines/mm diffraction grating was imprinted on the surface of solid silk materials by applying a 100-kPa pressure force at 60 °C for 60 s. Scanning electron microscopy and atomic force microscopy were used to evaluate the so-obtained microstructure. The surface after imprinting is shown in Fig. 2*D*, which illustrates the formation of periodic microstructures on the nanometer-smooth surfaces of the silk fibroin monoliths.

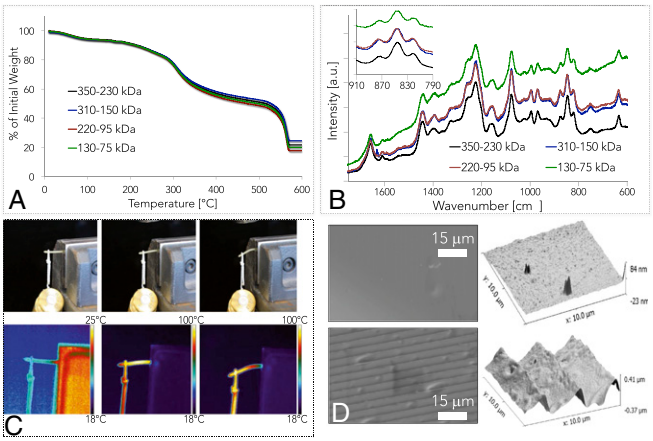

Fig. 2. Thermoplasticity of silk fibroin constructs. The semicrystalline nature of silk fibroin and the presence of free and bound water in the protein structure impart partial thermoplasticity to the solid material. (*A*) Thermogravimetric analysis was used to study the interplay between silk fibroin molecular weight and the residual water present in the solid material. Thermogravimetric curves of silk fibroin show an increase in free and bound water for materials with higher molecular weight. (*B*) Micro-Raman spectroscopy was used to investigate the presence of structural water in silk solid materials, as a function of molecular weight. Although the spectra of the protein did not present significant differences in the Raman shift as a function of molecular weight, the study of I_{850}/I_{830} ratio (*Inset*), which allows to study the hydrogen-bonding state of protein's tyrosine phenoxyl group, depicted a more hydrophobic tyrosine environment (higher I_{850}/I_{830} ratio) for higher protein molecular weights. (*C*) As a proof-of-concept of silk fibroin thermoplasticity, a dead load of 200 g has been applied to an end of a silk rod (Ø = 1 mm) that was secured at the opposite end with a bench vise. Thermograms of the experimental setup show that the increase of the rod internal temperature (heat was applied with a heat gun) above 80 °C causes a plastic deformation of the material. (*D*) Silk fibroin thermal reflow can also be used to imprint microstructures on the surface of the solid silk materials, by a combination of heat and pressure. For example, a diffraction grating can be imprinted on the surface of solid silk materials. Scanning electron micrographs and atomic force micrographs depicted the surface of a self-assembled silk fibroin construct before and after imprinting (60 °C, 60 s, 100 kPa) a periodic microstructure obtained from a diffraction grating. The material thermal reflow caused the formation of a grating structure on the surface of the silk fibroin construct.

The mechanical properties of self-assembled silk monoliths were investigated as a function of molecular weight (Fig. 3). Cylindrical specimens were evaluated through compression tests and compared with reference solid silk formats obtained through a previously reported method (35) involving the dissolution of freeze-dried, regenerated silk materials in hexafluoroisopropanol (HFIP) and the exposure of the so-formed xerogel to methanol solutions. Representative stress–strain curves of silk materials under uniaxial compression forces and compressive modulus of silk materials as a function of molecular weight are presented in Fig. 3 *A* and *B*, respectively. Silk fibroin materials with higher molecular weight showed a corresponding increase in the compressive modulus, as previously reported for other silk fibroin formats (i.e., films and sponges). The decrease in the mechanical properties for silk materials with lower molecular weight has been linked to a decreased formation of intermolecular hydrogen bonds and to less molecular entanglement. The silk fibroin blocks possessed a compressive modulus in the 2- to 6-GPa range. This value is almost an order or magnitude higher than the reported transverse compressive modulus for silk fibers (0.58 GPa) (36). This difference may originate from the highly

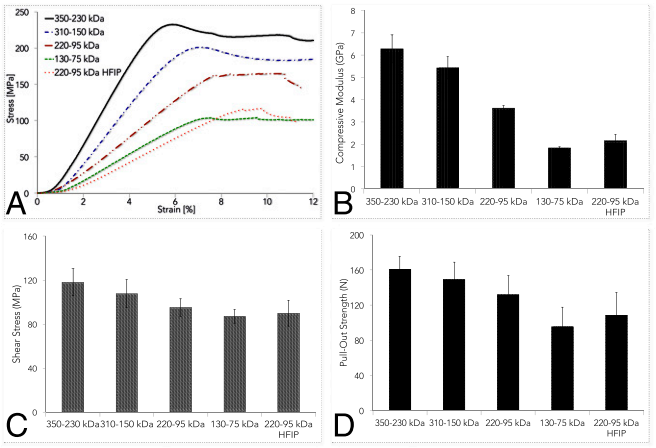

Fig. 3. Mechanical properties of silk fibroin solid materials. Cylindrical specimens were assessed through compression tests to evaluate the mechanical properties of silk fibroin monoliths as a function of molecular weight. Cylindrical silk fibroin specimen obtained through a HFIP-based process was used as reference material. (*A*) Representative stress–strain curves of silk materials under uniaxial compression forces. (*B*) Compressive modulus of silk materials as a function of molecular weight. To silk fibroin materials with higher molecular weight corresponded an increase in the compressive modulus. (*C*) Four-point bending test was also performed to evaluate the flexural strength of silk fibroin bars. Higher values of shear stress at failure were measured at increasing silk fibroin molecular weights. (*D*) Cylindrical specimen of silk fibroin of different molecular weights were machined in screws. The pull-out strength from a bone phantom was evaluated to test the biomechanical behavior of the material at the interface with a mineralized tissue phantom. The higher the molecular weight of silk fibroin, the higher the strength required to pull the screw out of the bone phantom.

anisotropic nature of silk fibers in their longitudinal direction that may impart inferior mechanical properties in the direction orthogonal to molecular alignment and by the different dimensions of the samples tested (silk fibers have a radius of ∼10 μm). Four-point bending test was also performed to evaluate the flexural strength of silk fibroin bars (Fig. 3*C*). Higher values of shear stress at failure were measured at increasing silk fibroin molecular weight, with measured flexural stress values in the order of 90–120 MPa. Silk fibroin fibers are renowned for their flexibility, which originates from the coordination of interfibrillar and intrafibrillar hydrogen bonds and from the molecular and nanoscale structure of the material that can be considered an amorphous matrix where crystalline β-sheet structures are embedded in highly ordered structures along the fiber's longitudinal axis (37). In the silk materials described in this study, the highly anisotropic nature of silk fibers is not maintained and the β-sheet nanocrystals are randomly oriented in the material, which impart a significant flexural strength comparable to some hierarchically structured tissues such as wet deer antler bone (38) or hard keratinaceous materials (39) (e.g., feather, claws, and nails). This remarkable similarity in the mechanical properties may be explained by a combination of (*i*) higher amount of free water in the tissues' structures (25–10 wt%) compared with <10 wt% of free water present in silk fibroin materials and (*ii*) higher porosity of the biological tissues that result in the formation of a less dense structure, even if the density of silk, keratin, and collagen is similar ($\rho \sim 1.3$–1.44 g/mL). Additionally, cylindrical specimens of silk fibroin of increasing molecular weights were machined and polished into various shapes to evaluate the performance of silk fibroin constructs once exposed to the mechanical forces and stress of commercial lathes and mechanical equipment (Fig. 4).

Specifically, for machined silk screws, the pull-out strength was evaluated in dry conditions at room temperature. The screws were fixed in polyurethane blocks, a metallic plate was attached to the screw head, and the fixture was extended in the tensile direction until failure, which occurred due to damage of the screw threading or of the shank. The higher the molecular weight of silk fibroin, the higher the strength required to pull the screw out of the attachment block, which corroborates the previously observed enhanced mechanical properties (i.e., compressive modulus and shear stress) with increasing molecular weights. In the future, modifications of hierarchical and second mesoscopic structures—determined during processing conditions—may also be applied to further control the mechanical performance of bulk silk constructs. Silk materials are subjected to swelling in water solutions, due to the formation of new hydrogen bonds with water molecules (17). Due to the relevance of swelling-induced geometrical changes for in situ application of silk 3D constructs at their final format, swelling ratio and water uptake (in percentage) were determined for silk fibroin screws of increasing molecular weight, in vitro. In accordance to what previously reported for silk materials fabricated via HFIP processing (35), silk fibroin screws had a swell ratio of ∼0.20 and a water uptake of ∼19 wt% after 72 h of hydration in PBS buffer. One-way ANOVA with Tukey's multiple-comparison test indicated that molecular weight was not statistically significantly affecting water uptake ($P > 0.05$). Additionally, it has been recently shown that silk screws specifically design for orthopedic applications can sustain human-mesenchymal stem cells attachment and differentiation toward osteogenic lineages while providing bio-inspired mechanical properties (40).

One of the most compelling attributes of operating in this context is to leverage protein assembly while embedding multiple functional elements in the reconstituted protein solution to generate functional material formats. The ability to further modify the assembled material with "top-down" approaches gives a wide array of utility for this class of naturally derived solid materials.

To demonstrate this potential, engineered silk fibroin constructs with embedded functionality were designed by hybridizing the structural protein with inorganic, organic, and biological compounds during monolith assembly (Fig. 4 *A* and *B*). The inclusion of gold nanorods in the silk fibroin liquid suspension enabled the formation of a light-responsive solid material that can be heated by illumination with a wavelength matching the plasmonic resonance of the nanorods (Fig. 4*C*). As an example, a silk fibroin screw fabricated with gold nanorods was heated up to 160 °C when exposed to 205 mW of diffuse infrared light (850 nm) emitted by a LED. In a second example, polydiacetylene (PDA) vesicles were added to silk fibroin suspensions at the point of material assembly to fabricate a hybrid material that can "transduce" internal strain with a colorimetric change (Fig. 4*D*) (4). The transducing mechanism was based on the intrinsic color change of PDA (from blue to red) produced by a conformational change in the PDA molecular structure under mechanical stimuli (which results in a more disordered, less coplanar, polymer with decreased bond conjugation length) (41). For this demonstration, silk fibroin–PDA monoliths were machined into a pin format. The pins undergo a blue-to-red chromatic transition when the force applied reaches the yield point of the

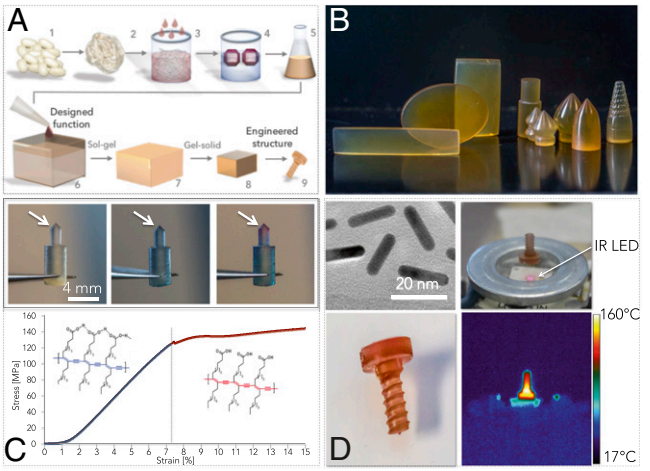

Fig. 4. Engineered silk fibroin constructs with designed functions. (*A*) By adding water-soluble molecules to the silk suspension at the point of material self-assembly, it is possible to impart designed functions to engineered silk fibroin materials. (*B*) Examples of engineered 3D silk constructs. (*C*) Polydiacetylene (PDA) vesicles may be added to silk fibroin suspensions at the point of material self-assembly to fabricate a hybrid material that transduces internal strain by colorimetric changes. For example, silk fibroin–PDA pins undergo to a blue-to-red chromatic transition when the force applied reaches the yield point of the material. (*D*) The inclusion of gold nanorods in silk fibroin enables the formation of a hybrid material that can be heated by applying a light that matches the plasmonic resonance of the nanoparticles. For example, a silk fibroin screw fabricated with gold nanorods can be heated up to 160 °C when exposed to the infrared light (850 nm) emitted by a LED.

material (Table 1). Finally, we demonstrate the doping and stabilization of silk fibroin with an enzyme [horseradish peroxidase (HRP)]. The addition of HRP results in the stabilization of the catalytic macromolecules that can then be released when the functional machined format is in contact with water solutions (Fig. 5*A*). HRP was incorporated in engineered silk screws and the release of the enzyme was evaluated as a function of time (Fig. 5*B*). Sustained release of the bioactive enzyme stabilized in silk fibroin was measured for 14 d in PBS at 37 °C (Fig. 5*C*). Thus, silk fibroin materials preserved the enzymatic activity of HRP in PBS at 37 °C for at least 14 d, compared with the nonencapsulated counterpart, which rapidly lost the 50% of its activity in ∼4 h. The mechanism of stabilization of water-soluble, heat-labile biological materials in silk proteins, has been described as a result of "protective barrier," "reduced mobility," and "microenvironment" effects (42). Silk fibroin forms a protective "shield" against environmental stresses for heat-labile molecules and provides dehydration and mitigation of oxidative stresses. In particular, a key role seems to be played by the formation of β-sheet structures; silk materials with increased β-sheet content provide an enhanced preservation medium for labile molecules (42). This phenomenon may be due to the decreased water content and the decreased diffusion coefficient of oxygen in silk materials with high β-sheet content (30). In terms of molecular weight, a correlation between average silk fibroin chain length and preservation of heat-labile molecules has not been clearly described in literature before. In this study, we have found that to higher molecular weight corresponded a statistically significant ($P < 0.05$) increase in the stability of the payload encapsulated in bulk silk materials. This may be due to the decreased diffusion coefficient of oxygen and the reduced amount of structural water in silk materials with an increased hydrophobicity (30). However, future studies are necessary to validate this speculation.

The ability to embed functional elements in biopolymers, control their self-assembly, and modify their ultimate form provides a compelling direction to help affect and redefine the hierarchical structure of natural materials and obtain durable, multifunctional mechanical formats. Managing self-assembly of silk allows to co-opt the bottom-up generative process to engineer function directly within end-material formats to obtain solids that include biological, optical, or chemical functionality and generate functional mechanical components that add utility to materials otherwise unattainable. The approach is applicable beyond the monolithic format presented here and underscores the opportunity provided by the combination of bottom-up and top-down fabrication approaches to empower bioinspired fabrication methods for compelling and high-performing multifunctional materials.

Experimental Procedures

Silk Monoliths Preparation. The all-water fabrication of silk fibroin monoliths requires three steps: (*i*) regeneration of silk fibroin in water solution; (*ii*) sol–gel transition of silk fibroin suspension; and (*iii*) gel–solid transition (i.e., fusion of the particles composing silk gel into monolithic constructs.

Silk fibroin regeneration. Cocoons from *Bombyx mori* were used as source of fibroin. Extraction of silk fibroin was achieved by standard degumming process, which involved boiling (t = 5–60 min) 2.5 g of chopped silk cocoons per L of 0.02 M sodium carbonate solution. By selecting the boiling time, it is possible to modulate the molecular-weight range of the regenerated silk fibroin, as previously described, albeit the polydispersity of silk fibroin increases, as the protein chains randomly degrade during the cooking of silk cocoons. Silk fibroin was then solubilized in 9.3 M lithium bromide for 4 h in a 60 °C oven. The chaotropic salt was subsequently removed through dialysis (3.5-kDa MWCO) against Milli-Q water for a total of 72 h, yielding an 8 wt% silk fibroin solution. The resulting SF solution was then purified by centrifugation at ∼12,700 × *g* over two 25-min-long periods, at a constant of 4 °C.

Sol–gel transition. Silk fibroin sol–gel transition was achieved with methods already reported in literature. In particular, the formation of silk fibroin hydrogel starting from solutions at 2–18 wt% was achieved through the following: spontaneous self-assembly by leaving silk fibroin suspension unperturbed for several weeks, slow evaporation of a concentrated silk fibroin suspension (12–18 wt%), and electrogelation.

Gel–solid transition. Gel–solid transition was achieved by exposing gels to air [either forced or still, relative humidity (RH) = 30%] at room temperature. In some cases, a mold made of semipermeable membrane (3.5-kDa MWCO) was used to maintain the silk gel with a defined shape.

Table 1. Strain-induced blue→red chromatic transition of silk–PDA composite materials as a function of protein molecular weight

Silk fibroin molecular weight, kDa	Strain-induced blue→red chromatic transition, %
350–230	5.68 ± 0.32
310–150	6.24 ± 0.77
220–95	7.59 ± 0.45
130–75	8.56 ± 0.82

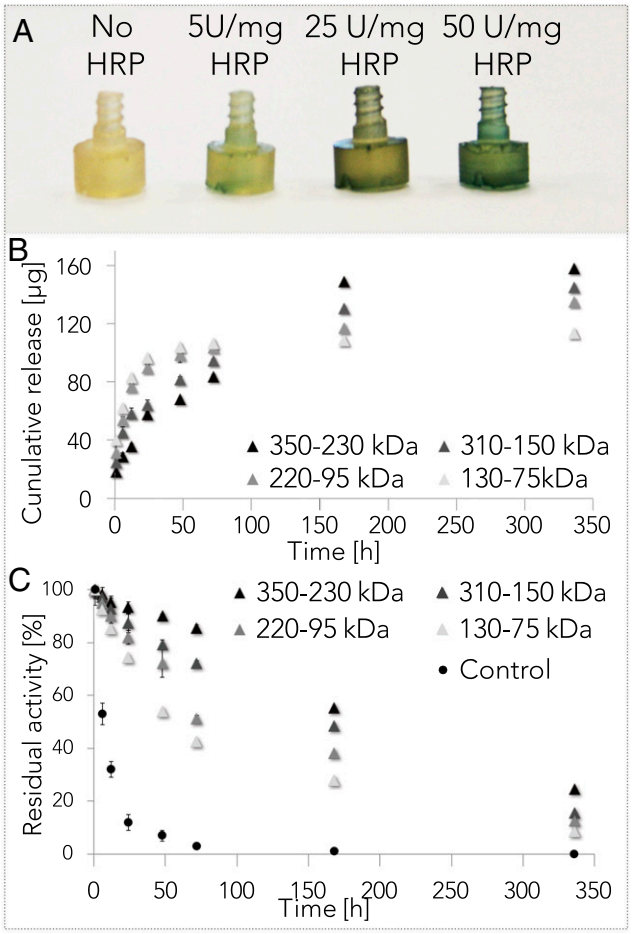

Fig. 5. Engineered silk fibroin screws with biological functions. (*A*) HRP was incorporated in engineered silk screws to impart catalytic activities to the material. The activity of the enzyme was evaluated with a chromogenic substrate that forms a blue precipitate upon reaction with the enzyme. (*B*) HRP cumulative release was investigated as a function of time. (*C*) A sustained release of the enzyme was measured for 14 d in PBS at 37 °C. Silk fibroin materials preserve the enzymatic activity of HRP in PBS at 37 °C by providing a controlled environment that protects the macromolecule from oxidative stress and hydrolysis. The residual activity of HRP stored in silk fibroin constructs was studied as a function of time and silk fibroin molecular weight. HRP not encapsulated in silk materials was used as control.

Materials Characterization. Details on the experimental methodologies used to fabricate silk-based composite monoliths, on the characterization of the morphological, physical, chemical, and mechanical properties of silk-based materials, and on statistical analysis may be found in *Supporting Information*.

ACKNOWLEDGMENTS. We acknowledge funding from the Office of Naval Research (Grant N00014-13-1-0596) for this work.

1. Rockwood DN, et al. (2011) Materials fabrication from *Bombyx mori* silk fibroin. *Nat Protoc* 6(10):1612–1631.
2. Brenckle MA, et al. (2013) Protein-protein nanoimprinting of silk fibroin films. *Adv Mater* 25(17):2409–2414.
3. Mitropoulos AN, et al. (2014) Synthesis of silk fibroin micro- and submicron spheres using a co-flow capillary device. *Adv Mater* 26(7):1105–1110.
4. Tao H, et al. (2015) Inkjet printing of regenerated silk fibroin: From printable forms to printable functions. *Adv Mater* 27(29):4273–4279.

5. Kim S, et al. (2014) All-water-based electron-beam lithography using silk as a resist. *Nat Nanotechnol* 9(4):306–310.
6. Kim S, et al. (2012) Silk inverse opals. *Nat Photonics* 6(12):817–822.
7. Omenetto F, Kaplan D (2008) A new route for silk. *Nat Photonics* 2(11):641–643.
8. Omenetto FG, Kaplan DL (2010) New opportunities for an ancient material. *Science* 329(5991):528–531.
9. Jin HJ, Kaplan DL (2003) Mechanism of silk processing in insects and spiders. *Nature* 424(6952):1057–1061.
10. Hagn F, et al. (2010) A conserved spider silk domain acts as a molecular switch that controls fibre assembly. *Nature* 465(7295):239–242.
11. Rising A, Johansson J (2015) Toward spinning artificial spider silk. *Nat Chem Biol* 11(5): 309–315.
12. Eisoldt L, Hardy JG, Heim M, Scheibel TR (2010) The role of salt and shear on the storage and assembly of spider silk proteins. *J Struct Biol* 170(2):413–419.
13. Hagn F, Thamm C, Scheibel T, Kessler H (2011) pH-dependent dimerization and salt-dependent stabilization of the N-terminal domain of spider dragline silk—implications for fiber formation. *Angew Chem Int Ed Engl* 50(1):310–313.
14. Rammensee S, Slotta U, Scheibel T, Bausch AR (2008) Assembly mechanism of recombinant spider silk proteins. *Proc Natl Acad Sci USA* 105(18):6590–6595.
15. Exler JH, Hümmerich D, Scheibel T (2007) The amphiphilic properties of spider silks are important for spinning. *Angew Chem Int Ed Engl* 46(19):3559–3562.
16. Vollrath F, Knight DP (2001) Liquid crystalline spinning of spider silk. *Nature* 410(6828):541–548.
17. Nguyen AT, et al. (2015) Crystal networks in silk fibrous materials: From hierarchical structure to ultra performance. *Small* 11(9-10):1039–1054.
18. Shulha H, Po Foo CW, Kaplan DL, Tsukruk VV (2006) Unfolding the multi-length scale domain structure of silk fibroin protein. *Polymer (Guildf)* 47(16):5821–5830.
19. Heim M, Keerl D, Scheibel T (2009) Spider silk: From soluble protein to extraordinary fiber. *Angew Chem Int Ed Engl* 48(20):3584–3596.
20. Hamley IW (2010) Liquid crystal phase formation by biopolymers. *Soft Matter* 6(9): 1863–1871.
21. Rey AD (2010) Liquid crystal models of biological materials and processes. *Soft Matter* 6(15):3402–3429.
22. Li G, et al. (2001) The natural silk spinning process. A nucleation-dependent aggregation mechanism? *Eur J Biochem* 268(24):6600–6606.
23. Leisk GG, Lo TJ, Yucel T, Lu Q, Kaplan DL (2010) Electrogelation for protein adhesives. *Adv Mater* 22(6):711–715.
24. Kim U-J, et al. (2004) Structure and properties of silk hydrogels. *Biomacromolecules* 5(3):786–792.
25. Mo C, Wu P, Chen X, Shao Z (2009) The effect of water on the conformation transition of *Bombyx mori* silk fibroin. *Vib Spectrosc* 51(1):105–109.
26. Monti P, Freddi G, Bertoluzza A, Kasai N, Tsukada M (1998) Raman spectroscopic studies of silk fibroin from *Bombyx mori*. *J Raman Spectrosc* 29(4):297–304.
27. Monti P, Taddei P, Freddi G, Asakura T, Tsukada M (2001) Raman spectroscopic characterization of *Bombyx mori* silk fibroin: Raman spectrum of silk I. *J Raman Spectrosc* 32(2):103–107.
28. Rousseau M-E, Lefèvre T, Beaulieu L, Asakura T, Pézolet M (2004) Study of protein conformation and orientation in silkworm and spider silk fibers using Raman microspectroscopy. *Biomacromolecules* 5(6):2247–2257.
29. Freddi G, Pessina G, Tsukada M (1999) Swelling and dissolution of silk fibroin (*Bombyx mori*) in *N*-methyl morpholine *N*-oxide. *Int J Biol Macromol* 24(2-3):251–263.
30. Marelli B, Brenckle MA, Kaplan DL, Omenetto FG (2016) Silk fibroin as edible coating for perishable food preservation. *Sci Rep* 6:25263.
31. Bressner JE, et al. (2014) Rapid fabrication of silk films with controlled architectures via electrogelation. *J Mater Chem B Mater Biol Med* 2(31):4983–4987.
32. Siamwiza MN, et al. (1975) Interpretation of the doublet at 850 and 830 cm^{-1} in the Raman spectra of tyrosyl residues in proteins and certain model compounds. *Biochemistry* 14(22):4870–4876.
33. Latza V, et al. (2015) Multi-scale thermal stability of a hard thermoplastic protein-based material. *Nat Commun* 6:8313.
34. Bier JM, Verbeek CJR, Lay MC (2014) Thermal transitions and structural relaxations in protein-based thermoplastics. *Macromol Mater Eng* 299(5):524–539.
35. Perrone GS, et al. (2014) The use of silk-based devices for fracture fixation. *Nat Commun* 5:3385.
36. Ko FK, et al. (2001) Engineering properties of spider silk. *Mater Res Soc Symp Proc* 702:U1.4.1.
37. van Beek JD, Hess S, Vollrath F, Meier BH (2002) The molecular structure of spider dragline silk: Folding and orientation of the protein backbone. *Proc Natl Acad Sci USA* 99(16):10266–10271.
38. Currey JD, et al. (2009) The mechanical properties of red deer antler bone when used in fighting. *J Exp Biol* 212(Pt 24):3985–3993.
39. Wang B, Yang W, McKittrick J, Meyers MA (2016) Keratin: Structure, mechanical properties, occurrence in biological organisms, and efforts at bioinspiration. *Prog Mater Sci* 76:229–318.
40. Li C, et al. (2016) Regenerated silk materials for functionalized silk orthopedic devices by mimicking natural processing. *Biomaterials* 110:24–33.
41. Kang DH, et al. (2012) Design of polydiacetylene-phospholipid supramolecules for enhanced stability and sensitivity. *Langmuir* 28(19):7551–7556.
42. Pritchard EM, Dennis PB, Omenetto F, Naik RR, Kaplan DL (2012) Review physical and chemical aspects of stabilization of compounds in silk. *Biopolymers* 97(6):479–498.
43. Nudelman F, et al. (2010) The role of collagen in bone apatite formation in the presence of hydroxyapatite nucleation inhibitors. *Nat Mater* 9(12):1004–1009.